Proceedings of IMECE2005
2005 ASME International Mechanical Engineering Congress and Exposition
November 5-11, 2005, Orlando, Florida, USA

IMECE2005-80012

RADIATION TRANSFER IN WHISPERING-GALLERY MODE MICROCAVITIES

Haiyong Quan
Dept. of Mechanical and Aerospace Engineering
Rutgers, The State University of New Jersey
Piscataway, NJ 08854, USA
hyquan@eden.rutgers.edu

Zhixiong Guo
Dept. of Mechanical and Aerospace Engineering
Rutgers, The State University of New Jersey
Piscataway, NJ 08854, USA
Corresponding author: guo@jove.rutgers.edu

ABSTRACT

Micro/nanoscale radiation transfer in whispering-gallery mode (WGM) microcavities is investigated. Each cavity consists of a waveguide and a microdisk coupled in a planar chip. In order to characterize the WGM resonance phenomena, studies of configuration parameters, specifically the microdisk size, the gap distance separating the microdisk and waveguide, and the waveguide width are numerically conducted. The finite element method is used for solving Maxwell's equations which govern the propagation of electromagnetic (EM) field and the radiation energy transport in the micro/nanoscale WGM structures. The EM fields and the radiation energy distributions in the microcavities are then obtained. The scattering spectra for three different microdisk sizes are also obtained; and through which the WGM resonant properties such as the quality factor, the full-width at half maximum (FWHM), the free spectral range, and the finesse of the resonant modes are analyzed. It is found that the resonant frequencies and their free spectral ranges are predominantly determined by the size of the microcavity; while the FWHM, finesse, and quality factor are strong functions of the gap.

INTRODUCTION

The term whispering-gallery mode describes the resonance of photons that circulate around the inner surface of a dielectric medium of circular geometry as a result of total internal reflection (TIR).[1] With size flexibility, mechanical stability, adaptability to integrated circuits, very high quality factor (Q value), and very small mode volume at optical frequencies, WGM microcavities are widely used for basic research and for applications. Stemming from extensive studies of Mie resonance in small particles,[2] further studies are focusing on microspheres of fused silica with high-Q WGMs as a novel type of optical resonator. $Q > 10^9$ has been demonstrated at near-infrared and red wavelengths.[3] An important application of this cavity quantum electrodynamic effect involves miniature lasers.[4,5] Other applications include high resolution spectroscopy,[6] and optical biosensors,[7,8] etc. Modes of this type possess negligible electrodynamically defined radiative losses, and are not accessible by free-space beams; and therefore, require employment of near-field coupler devices. At present, in addition to the well-known prism coupler with frustrated TIR, coupler devices include side-polished fiber couplers[9] and fiber tapers.[10] The principle of all these devices is based on providing efficient energy transfer to the resonant circular TIR guided wave in the resonator through the evanescent field of a guided wave or a TIR spot in the coupler.

The advances in micro/nano-fabrication techniques have made it feasible to consider WGM optical resonators having physical dimensions of the order of optical wavelengths. Semiconductor WGM microcavities such as microdisks, microrings, and microcylinders can be easily miniaturized to a few microns in diameter, while maintaining a high Q. They have attracted considerable attention in the literature, as they are promising ultracompact building blocks for add-drop filters,[11] microlasers,[12] all-optical switches,[13] and sensing applications;[14] and they open the route to a large area reduction of complex integrated photonic devices.[15]

In recent years, WGM optical biosensors[7,8] have been studied as a research field of attractive interest because of the great need in life sciences, drug discovery, and recent worldwide protection from the threat of chemical and bio-terrorism. Usually the optical resonance techniques can be used to enhance the sensitivity of biosensor devices.[16] The WGM miniature sensor possesses high sensitivity, small sample volume, and robust integrated property to make a lab-on-a-chip device and may be used to identify and monitor proteins, DNA, and toxin molecules. They can detect as few as 100 molecules as reported by Boyd and Heebner.[14]

In order to optimize the sensitivity of WGM based sensors, we must understand the micro/nanoscale radiation transfer and radiation-matter interactions in the evanescent field. Experimental methods for conducting such a task are generally time-consuming and costly. Analytical models[2] have been introduced to analyze optical resonant phenomena associated with small particles, such as the perturbation model.[17] Analytical solutions are very useful and powerful in understanding the physical essence of the phenomena. Although they can reveal the individual intuitive resonance properties of a microcavity, it is hard for them to capture a completely real picture of a sensor as a system. For example, a perturbation theory is hardly able to account for the coupling of the evanescent fields in the nanoscale gap and the interactions of the resonator with surrounding individual molecules. As a matter of fact, the evanescent field in the microcavity is very sensitive against the gap through which photons tunnel. The Mie theory cannot describe well the photon tunneling effect. A complete modeling of the EM and radiation field in the whole WGM structure is highly desired.

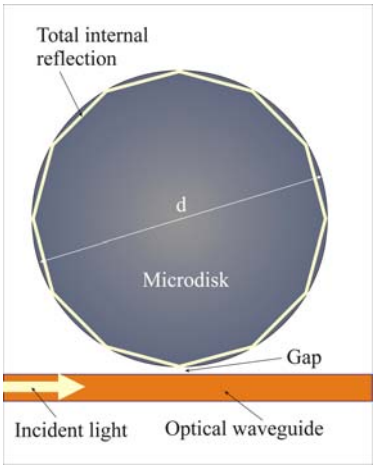

Figure 1. Sketch of a WGM microcavity.

Previously many WGM-based sensors have a structure of a microsphere and an eroded optical fiber coupling design. Although the *Q*-value for a microsphere-based resonator can be very high, such a configuration may have some flaws for use as an ideal sensor. For instance, mass manufacturing of such devices can be difficult; and non-uniformity exists, especially in the control of the gap distance separating the light-delivery fiber and the resonator. The gap is a critical parameter for photon tunneling and may affect the *Q*-value and resonant frequencies.

Here we consider sensors of a planar waveguide and microdisk coupling structure as shown in Fig. 1. Such devices can be manufactured on silicon-based thin films using conventional silicon integrated circuits (IC) processing with high uniformity and density. This cavity structure will further reduce the sensor size and enhance miniaturization of the devices. Planar WGM sensors possess high sensitivity, small sample volume, and robust integrated property for system-on-a-chip applications.

Maxwell's equations can be used to describe the radiation transfer in WGM microcavity systems. More than 30 years ago, Silvester[18] developed high order Lagrange elements and first applied the finite element method (FEM) for solving the EM field problems. The present authors[19] successfully applied the FEM to simulate the EM and radiation energy fields in WGM resonators consisting of a microsphere and an optical fiber.

In this report, parametric studies through FEM simulations are made of the waveguide-microdisk coupling WGM microcavities. The operating resonant frequencies are chosen in the near infrared range, which is ideal for biomaterials and biomolecules. The parameters selected for study include the diameter of the microdisk, the gap distance separating the waveguide and microdisk, and the width of the waveguide. Their effects on the WGM resonant phenomena will be scrutinized. The characteristics of the EM field and radiation energy storage in the WGM resonators will be investigated.

MODELING

WGM resonance inside the microdisk is typically an equatorial brilliant ring, and this ring is located on the same plane as the waveguide. Further, the structure of the microcavities is planar. So it is feasible to use a two-dimensional (2-D) theoretical model. The time-dependent Maxwell's equations are

$$\begin{cases} \nabla\cdot\bar{E}=\dfrac{\rho}{\varepsilon};\quad \nabla\times\bar{E}=-\mu\dfrac{\partial\bar{H}}{\partial t} \\ \nabla\cdot\bar{H}=0;\quad \nabla\times\bar{H}=\bar{J}+\varepsilon\dfrac{\partial\bar{E}}{\partial t} \end{cases} \tag{1}$$

where $\bar{E}$ and $\bar{H}$ are the electric and magnetic field vectors, respectively; ε and μ are the permittivity and permeability of the medium; ρ is the electric charge density; and $\bar{J}$ is the electric current density.

For the electric field, since $\rho=0$ and $\bar{J}=\sigma\bar{E}$, we can derive the equation for $\bar{E}$ as follows:

$$\nabla^2\bar{E}-\mu\sigma\frac{\partial\bar{E}}{\partial t}-\mu\varepsilon\frac{\partial^2\bar{E}}{\partial t^2}=0 \tag{2}$$

where σ is the electrical conductivity. We can transfer the above equation to the form of a time-harmonic wave by setting $\bar{E}(\bar{r},t)=\bar{E}_0(\bar{r})e^{i\omega t}$. The coupled set of Maxwell's equations is then reduced to a simple form:

$$\frac{1}{\mu}\nabla^2\bar{E}+\omega^2\varepsilon_c\bar{E}=0;\quad \frac{1}{\mu}\nabla^2\bar{H}+\omega^2\varepsilon_c\bar{H}=0 \tag{3}$$

where we have introduced the complex permittivity $\varepsilon_c = \varepsilon_{cr} \cdot \varepsilon_0 = \varepsilon - i(\sigma/\omega)$ and $\omega = 2\pi c/\lambda$; c is the speed of light in the medium and λ is the light wavelength. Here, the complex index of refraction, $m = n - ik$, is conveniently introduced for the treatment of wave propagation; n is the real part of the refractive index and represents a spatial phase change of the electromagnetic wave; k is the absorption index and stands for a spatial damping on the electromagnetic wave. The relationship between ε_{cr} and m is expressed by $\varepsilon_{cr} = m^2 = n^2 - k^2 - i2nk$.

In the present study we consider the In-plane TE waves, where the electric field has only a z-component; and it propagates in the x-y plane. Thus, the fields can be written as:

$$\begin{aligned} \bar{E}(x,y,t) &= E_z(x,y)\bar{e}_z e^{i\omega t} \\ \bar{H}(x,y,t) &= [H_x(x,y)\bar{e}_x + H_y(x,y)\bar{e}_y]e^{i\omega t} \end{aligned} \quad (4)$$

At the interface and physical boundaries, the natural continuity condition is used for the tangential component of the magnetic field, i.e., $\bar{n} \times \bar{H} = 0$. For the outside boundaries, the low-reflecting boundary condition is adopted. The low-reflecting means that only a small part of the wave is reflected, and that the wave propagates through the boundary almost as if it were not present. This condition can be formulized as $\bar{e}_z \cdot \bar{n} \times \sqrt{\mu}\bar{H} + \sqrt{\varepsilon}E_z = 0$. The light source term E_{0z}, which propagates inwards through the entry of the waveguide, was treated as an electrically low-reflecting boundary expressed by $\bar{e}_z \cdot \bar{n} \times \sqrt{\mu}\bar{H} + \sqrt{\varepsilon}E_z = 2\sqrt{\varepsilon}E_{0z}$.

The WGM resonances possess very high quality factors due to minimal reflection losses. The quality factor Q is defined as a ratio of 2π stored energy to energy lost per cycle. From the energy conservation and resonance properties, we can deduce a simple approximate expression:[20] $Q = \omega_0/\Delta\omega = 2\pi\omega_0\tau$, where ω_0 is the resonant frequency, $\Delta\omega$ is the resonance linewidth, and τ is the photon lifetime.

From Maxwell's equations, we can derive the energy conservation equation to describe the resistive and radiative energy, or energy loss, through Poynting's theorem:[21]

$$\oint_S (\bar{E} \times \bar{H}) \cdot \bar{n} dS = -\int_V \left(\bar{E} \cdot \frac{\partial \bar{D}}{\partial t} + \bar{H} \cdot \frac{\partial \bar{B}}{\partial t} \right) dV - \int_V \bar{J} \cdot \bar{E} dV \quad (5)$$

where V is the computation domain and S is the closed boundary of V. The term on the left had side of the above equation represents the radiative losses. The quantity $\bar{S} = \bar{E} \times \bar{H}$ is called as the Poynting vector. The first integral on the right hand side represents the rate of change in total energy. The second integral on the right hand side represents the resistive losses that result in heat dissipation in metallic materials.

For dielectric materials, however, $\bar{J} = 0$. Under the assumption that the material is linear and isotropic, we have constitutive relations as follows:

$$\begin{aligned} \bar{E} \cdot \frac{\partial \bar{D}}{\partial t} &= \varepsilon \bar{E} \cdot \frac{\partial \bar{E}}{\partial t} = \frac{\partial}{\partial t}\left(\frac{1}{2}\varepsilon \bar{E} \cdot \bar{E}\right) \\ \bar{H} \cdot \frac{\partial \bar{B}}{\partial t} &= \frac{1}{\mu}\bar{B} \cdot \frac{\partial \bar{B}}{\partial t} = \frac{\partial}{\partial t}\left(\frac{1}{2\mu}\bar{B} \cdot \bar{B}\right) \end{aligned} \quad (6)$$

So the formula of Poynting's theory is simplified to

$$\oint_S (\bar{E} \times \bar{H}) \cdot \bar{n} dS = -\frac{\partial}{\partial t}\int \left(\frac{1}{2}\varepsilon \bar{E} \cdot \bar{E} + \frac{1}{2\mu}\bar{B} \cdot \bar{B} \right) dV \cdot \quad (7)$$

This formula shows us that the change in total energy of electromagnetic field is totally converted to radiative energy. There is no heat dissipation in this condition. However, actual dielectric materials are dispersive (absorbing) media, and exhibit energy losses because the presence of dispersion in general signifies a dissipation of energy.

To discuss dispersion, let us consider an electromagnetic field of a single frequency. The differential form of equation (7) is expressed as $\nabla \cdot (\bar{E} \times \bar{H}) = -(\bar{E} \cdot \frac{\partial \bar{D}}{\partial t} + \bar{H} \cdot \frac{\partial \bar{B}}{\partial t})$, in which the steady rate of change of the energy is the mean quantity of heat evolved per unit time and volume.

Supposing $\bar{E}$ and $\bar{D}$ are complex numbers for a field of a single frequency, we substitute $(\bar{E} + \bar{E}^*)/2$ and $(-i\omega\varepsilon\bar{E} + i\omega\varepsilon^*\bar{E}^*)/2$ for $\bar{E}$ and $\partial\bar{D}/\partial t$ respectively [$\bar{D}^* = \varepsilon^*\bar{E}^*$ and $\bar{E}(\bar{r},t) = \bar{E}_0(\bar{r})e^{-i\omega t}$], and similarly for $\bar{H}$ and $\partial\bar{B}/\partial t$. After averaging with respect to time over the period $2\pi/\omega$, the products $\bar{E} \cdot \bar{E}$ and $\bar{E}^* \cdot \bar{E}^*$, which contain factors $e^{\mp 2i\omega t}$, give zero, leaving the rate of change in electromagnetic energy as

$$\begin{aligned} \nabla \cdot \vec{q} &= (\bar{E} \cdot \frac{\partial \bar{D}}{\partial t} + \bar{H} \cdot \frac{\partial \bar{B}}{\partial t}) = \frac{i\omega}{4}[(\varepsilon^* - \varepsilon)\bar{E}_0 \cdot \bar{E}_0 + (\mu^* - \mu)\bar{H}_0 \cdot \bar{H}_0] \\ &= \frac{\omega}{2}(\varepsilon'' \bar{E}_0 \cdot \bar{E}_0 + \mu'' \bar{H}_0 \cdot \bar{H}_0) \end{aligned} \quad (8)$$

where ε'' and μ'' are the imaginary parts of ε and μ. The energy loss should be positive since the dissipation of energy is accompanied by the evolution of heat (under the law of increase of entropy). It hints that the imaginary parts of ε and μ are always positive for all substance and at all frequencies.

The finite element method is employed to simulate the EM and radiation field and the details of the method are available in Quan and Guo[19]. Thus, the description is not repeated here. The commercial software FEMLAB was used for the finite element solution and for pre- and post-processing. A typical simulation domain is a 20μm × 25μm rectangular area with a centered microdisk. The length of the waveguide

is extended to the edge of the simulation domain. A laser beam from a tunable continuous-wave (CW) laser is coupled into the left end of the waveguide to excite the resonance. The frequency of the incident laser varies between 365 THz (822nm) and 375 THz (800nm). In the nanometer scaled gap separating the waveguide and microdisk, photons tunnel and the light will cross the gap and enter into the microdisk. When the frequency of the input light is the same as the natural resonant frequency of the system, WGM phenomenon occurs. At the resonant frequency, the scattering intensity from the microdisk will increase sharply and form a peak in the intensity-frequency spectrum.

In the simulations, the model geometry is meshed by 51,400 triangle elements. The software automatically scales down the domain into different spatial levels to generate fine meshes around the physically sensitive regions, like the gap and the waveguide. Since the resonant rings are usually located in a thin layer beneath the cavity surface, we manually scale the cavity into two regions such that the meshes in the ring area can be further refined. The general computational resolution of wavelength is 0.5nm, but special attention is paid to the resonance frequencies where 0.01nm resolution is adopted. To conduct parametric studies, the diameter of the microdisk varies between 10 and 15μm. The width of the waveguide changes between 2 and 3μm. The gap between the microdisk and the waveguide varies between 100 to 300nm. Both the microdisk and the waveguide are made from silicon nitride (Si_3N_4) whose refractive index is 2.01 against the operating wavelength.

RESULTS AND DISCUSSION

First we try to demonstrate the EM fields and radiation energy distributions in the WGM microcavities. Figures 2 and 3 illuminate the distributions of the electric field and the radiation energy, respectively, for a microcavity of 15μm in diameter. Three different cases under off-resonance, the first-order resonance, and the second-order resonance are selected for comparison. The first- and second-order resonance frequencies were found at 373.78 THz (λ=802.61nm) and 372.96 THz (804.37nm), respectively, when the surrounding medium was air. The off-resonance frequency was selected at 372.67 THz (λ=805nm). The gap which is defined as the smallest distance between the waveguide and microdisk is 230nm and the width of the waveguide is 2μm. These are the general data in the computations if not specified otherwise.

From Fig. 2, it is clearly observed that the EM field exists in the microdisk no matter there is a WGM resonance or no resonance. Thus, photons tunnel from the waveguide to the microdisk because the gap distance is less than one wavelength. Under the first-order resonance, a brilliant ring in the EM field is formed inside the microdisk in the vicinity close to the peripheral surface. While under the second-order resonance, there are two bright rings inside the microdisk. The EM field in the internal ring is stronger than that in the outer ring. For the EM field in the waveguide, however, the off-resonance case has the strongest strength and the first-order resonance case has the weakest strength.

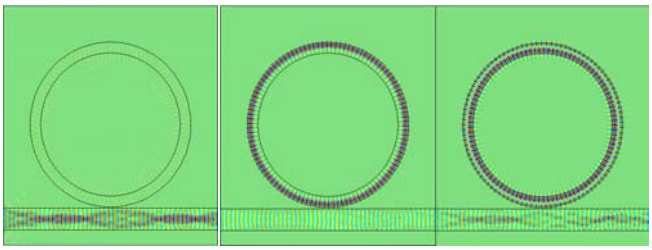

Figure 2. Electric field distributions under off-resonance, the first-order resonance, and the second-order resonance (from left to right) for a microcavity of 15μm in diameter.

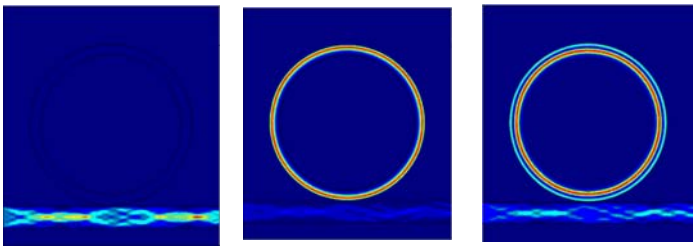

Figure 3. Energy distributions under off-resonance, the first-order resonance, and the second-order resonance (from left to right) for a microcavity of 15μm in diameter.

From Fig. 3, it is seen that the microdisk and waveguide coupling resonator has a very strong energy storing property in the resonator when WGMs occur. The majority energy stores in the thin ring close to the peripheral surface of the microdisk for the first-order resonance. For the second-order resonance, the energy is mostly stored in the internal ring. However, there still exists an outer ring which is thin and weak as compared with the internal ring. Thus, the scattering intensity from the microdisk surface under the second-order resonance is expected to be weaker than that under the first-order resonance. For the case of off-resonance, the energy is confined inside the waveguide and energy storage in the resonator is almost invisible. The ratio of the radiation energy storing in the microdisk to the radiation energy passing through the waveguide is 10.5 for the first-order resonance shown in Fig. 3, whereas it is only 0.008 for the case of off-resonance. The microdisk can absorb and store the majority of the radiation energy when WGM resonance occurs. This leads to the enhancement of the evanescent radiation field around the periphery of the resonator, where sensitivity to any external perturbation is maximal.

Figures 4 and 5 show the first-order resonance electric field and radiation energy distribution for microcavities of 10μm in diameter and 5μm in diameter, respectively. The resonance frequency is 377.44 THz (λ=801.198nm) for the microcavity of 10μm in diameter, and 371.65 THz (λ=807.213nm) for the microcavity of 5μm in diameter. It is seen that the resonance mode of the small disk is confined in a smaller room and occupies more relative area than the large one. However, the ratio of the radiation energy storing in the disk to the radiation energy passing through the waveguide is 13.5 for the 10um-in-diameter microcavity and 5.3 for the small disk. This phenomenon results from the compatibility of disk and waveguide. In both two simulation cases, we kept the width of waveguide and only reduced the size of disk, i.e., the incident energy flux is fixed. The energy storage capacity of the small disk was saturated at this energy flux in the 2μm wide waveguide. The way to solve this problem is to reduce the width of the waveguide to a well compatible range with the disk. After reducing the width to 0.5μm, the ratio of the radiation energy storing in the small disk to the radiation energy passing through the waveguide rises to 32.9. Thus, the waveguide width affects the energy coupling efficiency.

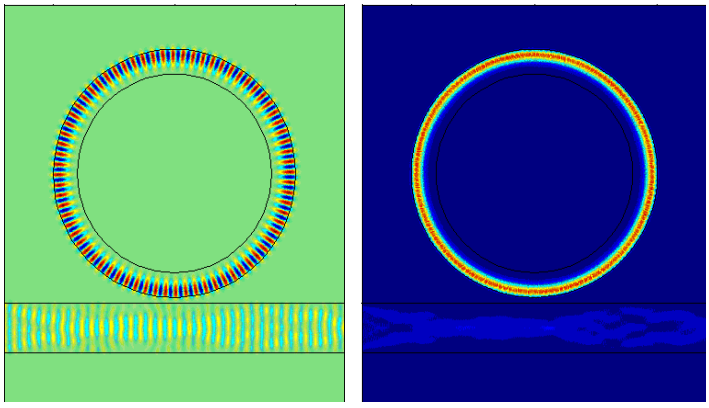

Figure 4. Electric field and energy distribution of the first-order resonance for the microcavity of 10μm in diameter.

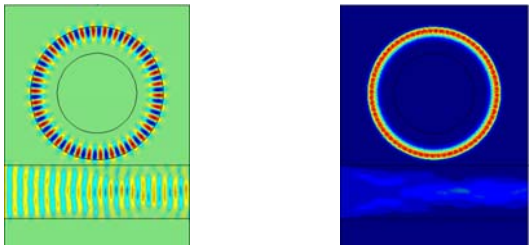

Figure 5 Electric field and energy distribution of the first-order resonance for the microcavity of 5 μm in diameter.

The resonator configuration parameters like the microdisk size, the gap between the waveguide and microdisk, and the width of the waveguide certainly affect the resonance phenomena and signal intensity. To investigate the parametric influences, we obtained the scattering spectra of radiation energy outflow (Poynting's vector from the microdisk peripheral surface) with varying excitation frequencies between 365 THz and 375 THz for different microdisk diameters, gap distances, and waveguide widths, respectively. Figure 6 shows the scattering spectra for three different microdisk diameters: 10μm, 12.5μm, and 15μm. The width of the waveguide and the gap between the waveguide and microdisk are fixed at 2μm and 230nm, respectively. The resonance data retrieved from these scattering spectra are listed in Table 1. The parameters include the resonant frequency and its corresponding wavelength, the quality factor, the full-width at half maximum (FWHM) of the resonant frequency band, the resonant frequency interval represented by the free-spectral range (FSR, = periodicity of resonance peaks), and the finesse of the resonant mode defined as F = FSR/FWHM. Three first-order resonant frequencies (modes) were found for each of the cases in the frequency range considered.

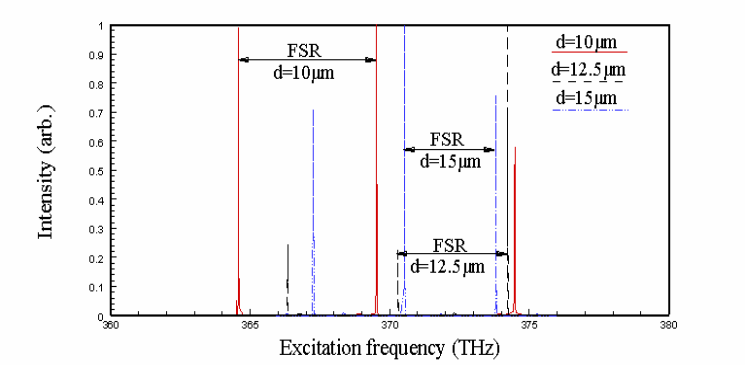

Figure 6. Scattering spectra for different microdisk sizes of d = 10μm, 12.5μm, and 15μm, respectively.

Since both the gap and waveguide width do not affect the resonance modes, it is not easy to find differences in the scattering spectra for different gap distances and waveguide widths. Figures 7 and 8 portray the gap and waveguide width effects, respectively, on the WGM resonant frequencies, the corresponding FWHM and FSR, and the quality factor *Q*. All the data were retrieved from the respective scattering spectra and are listed in Table 1. Four different gap distances of 100nm, 200nm, 230nm, and 300nm, and three different waveguide widths of 2.0μm, 2.5μm, and 3.0μm were considered. The surrounding medium was air for all simulation conditions. There are three whispering-gallery modes (RF-1, RF-2, and RF-3) in the frequency range considered, and each mode has its own FWHM and Q values.

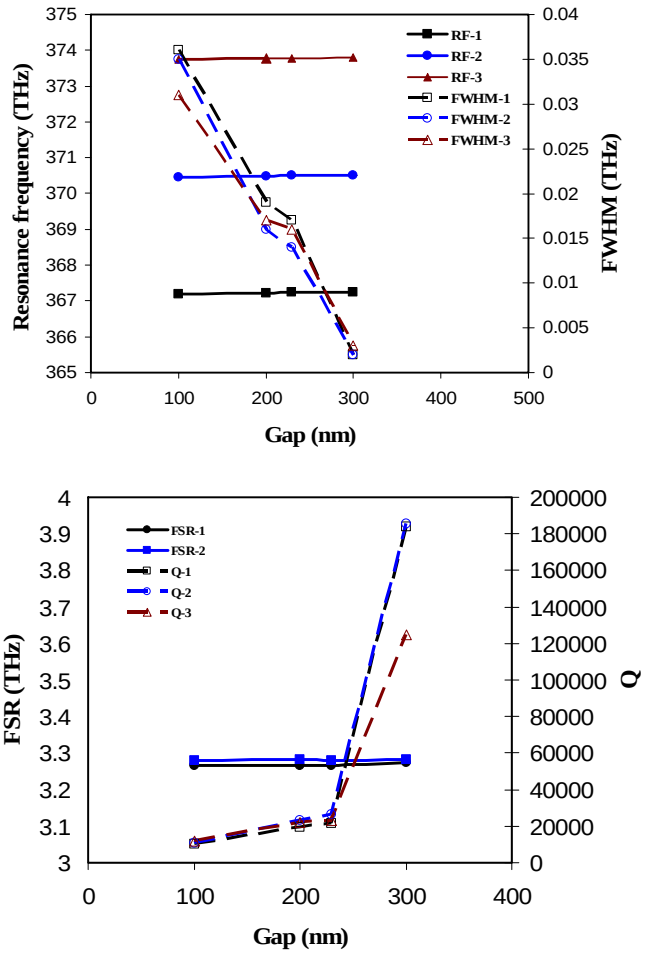

Figure 7. Effects of the gap on the WGM resonant frequencies, FWHM, FSR, and quality factor *Q*.

From Figs. 6 to 8 and Table 1, it is found that the microdisk size affects significantly the resonant frequencies and their intervals. The FSR value increases with the decrease of the diameter of the microdisk. However, the microdisk size does not appreciably influence the quality factor and the finesse. On the other hand, the gap and the waveguide width do strongly affect the quality factor and the finesse of the WGM. But the gap has a slight effect on the resonant frequencies and the FSR, and the influence of the waveguide width on the resonant frequencies and the FSR is negligible. The decrease of the gap results in a broadening in the FWHM of the resonant frequency band, and consequently reduces the quality factor and the finesse of the resonant frequencies. The wider is the waveguide, the larger are the quality factor and the finesse of the resonant modes. The quality factors of these resonant modes are varying between 10,200 and 185,255 in the present studies. The finesse of these resonance modes is in a range from 92.0 to 1637.5. The FSR of the resonant modes for the 15μm-diameter microdisk are slightly varying between 3.266 THz and 3.281 THz for all the specified gap distances and waveguide widths. Thus, the WGM frequencies are predominantly determined by the microdisk diameter. The gap distance and the waveguide width affect mainly the resonance quality.

Table 1. Resonance data from the scattering spectra.

Resonance frequency f_R (THz)	Excitation Wavelength λ_R (nm)	Quality factor Q	FWHM (THz)	FSR (THz)	Finesse F
d = 10.0μm, g = 230nm, w = 2.0μm					
364.582	822.86	21,446	0.017	4.944	282.5
369.526	811.85	20,529	0.018		
374.490	801.09	22,029	0.017	4.964	283.6
d = 12.5μm, g = 230nm, w = 2.0μm					
366.321	818.53	22,895	0.016	3.931	253.6
370.252	810.26	24,683	0.015		
374.201	801.71	22,011	0.017	3.949	246.8
d = 15.0μm, g = 230nm, w =2.0μm					
367.235	816.92	21,602	0.017	3.266	210.7
370.501	809.72	26,464	0.014		
373.780	802.61	23,361	0.016	3.279	218.6
d = 15.0μm, g = 100nm, w = 2.0μm					
367.197	817.00	10,200	0.036	3.267	92.0
370.464	809.79	10,585	0.035		
373.743	802.69	12,056	0.031	3.279	99.4
d = 15.0μm, g = 200nm, w = 2.0μm					
367.224	816.94	19,328	0.019	3.267	186.7
370.495	809.73	23,155	0.016		
373.776	802.63	21,987	0.017	3.281	198.8
d = 15.0μm, g = 300nm, w = 2.0μm					
367.235	816.91	183,617	0.002	3.275	1,637.5
370.510	809.70	185,255	0.002		
373.791	802.59	124,597	0.003	3.281	1,312.4
d = 15.0μm, g = 200nm, w = 2.5μm					
367.215	816.96	26,230	0.014	3.277	211.4
370.492	809.73	21,794	0.017		
373.765	802.64	23,360	0.016	3.273	198.4
d = 15.0μm, g = 200nm, w = 3.0μm					
367.217	816.96	40,802	0.009	3.271	344.3
370.488	809.74	37,049	0.010		
373.764	802.65	46,721	0.008	3.276	364.0

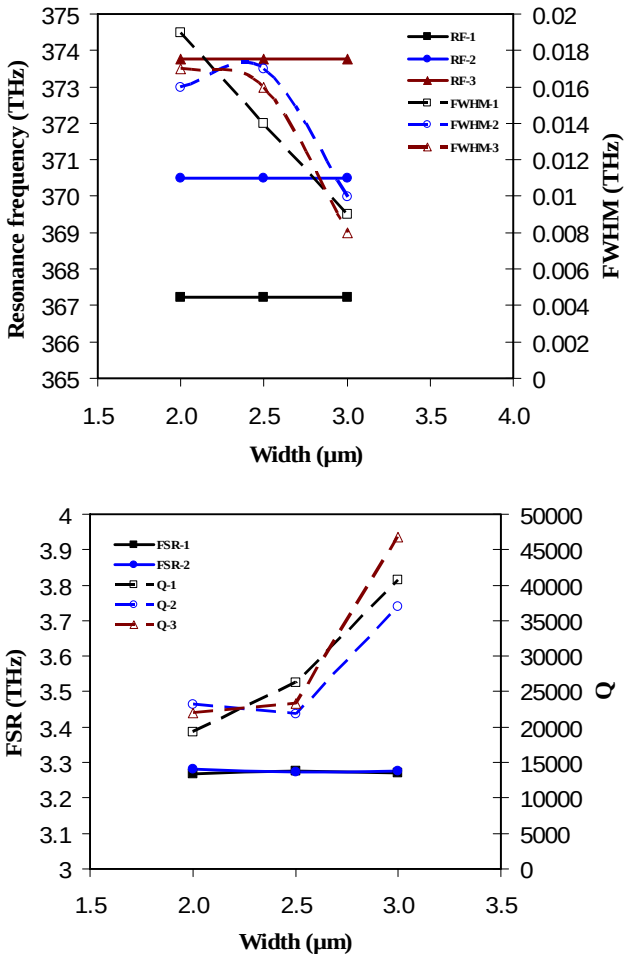

Figure 8. Effects of the waveguide width on the WGM resonant frequencies, FWHM, FSR, and quality factor *Q*.

CONCLUSIONS

The radiation transfer and resonant phenomena in waveguide-microdisk coupling WGM microcavities were investigated. The time-dependent Maxwell's equations were utilized for describing the EM field and radiation transfer, and solved by the finite element method. The EM field and the radiation energy distribution in three different sizes of microcavities were shown. When WGM resonance occurs, photon tunneling from the waveguide to the cavity is greatly enhanced and significant radiation energy is stored in the microcavity. The energy storage capability depends not only on the cavity size, but also on the compatibility of the waveguide. Parameters like the microdisk size, the gap separating the microdisk and waveguide, and the waveguide width all affect the radiation transfer and resonant phenomena. The WGM resonant frequencies and their intervals are predominantly determined by the microdisk diameter. The gap and the waveguide size have little effect on the resonant frequencies and their intervals. However, the gap as well as the waveguide width does strongly influence the qualify factor and the finesse of the resonant modes. In particular, the gap effects should not be overlooked. An optimal gap may exist for photon tunneling under WGM resonances.

ACKNOWLEDGMENTS

Z. Guo acknowledges the partial support of an Academic Excellence Funds Award from Rutgers University and an NSF grant (CTS-0541585) to the project. The project support from the New Jersey Nanotechnology Consortium at Bell Labs/Lucent Technologies is also appreciated.

REFERENCES

1. H.M. Nussenzveig, Diffraction effects in semiclassical scattering, Cambridge University Press, New York (1992).
2. P.W. Barber and P.K. Chang, Optical effects associated with small particles, World Scientific, Singapore; New Jersey; Hong Kong (1988).
3. M.L. Gorodetsky, A.A. Savchenkov, and V.S. Ilchenko, "Ultimate Q of optical microsphere resonators," Opt. Lett., 21, 453-455 (1996).
4. M. Cai, Q. Painter, K.J. Vahala, and P.C. Sercel, "Fiber-coupled microsphere laser", Opt. Lett., 25, 1430-1432 (2000).
5. S.M. Spillane, T.J. Kippenberg, and K.J. Vahala, "Ultralow-threshold Raman laser using a spherical dielectric microcavity," Nature, 415, 621-623 (2002).
6. S. Schiller, and R.L. Byer, "High-resolution spectroscope of whispering gallery modes in large dielectric spheres," Opt. Lett., 16, 1138-1140 (1991).
7. F. Vollmer, D. Braun, A. Libchaber, M. Khoshsima, I. Teraoka, and S. Arnold, "Protein detection by optical shift of a resonant microcavity", Appl. Phys. Lett., Vol. 80, No. 21, pp. 4057-4059 (2002).
8. S. Arnold, M. Khoshsima, I. Teraoka, and F. Vollmer, "Shift of whispering-gallery modes in microspheres by protein adsorption", Opt. Lett., 28, 272-274 (2003).
9. A. Serpenguzel, S. Arnold, and G. Griffel, "Excitation of resonances of microspheres on an optical fiber," Opt. Lett., 20, 654-656 (1995).
10. J.C. Knight, G. Cheung, F. Jacques, and T.A. Birks, "Phase-matched excitation of whispering gallery mode resonances using a fiber taper," Opt. Lett., 22, 1129-1131 (1997).
11. B.E. Little, S.T. Chu, H.A. Haus, J. Foresi, and J.P. Laine, "Microring resonator channel dropping filters", J. Lightwave Tech., 15, 998-1005 (1997).
12. F.C. Blom, D.R. van Dijk, H.J Hoekstra, A. Driessen, and T.J.A. Popma, "Experimental study of integrated-optics

micro-cavity resonators: toward an all-optical switching device," Appl. Phys. Lett., 71, 747-749 (1997).

13. A.F.J. Levi, R.E. Slusher, S.L. McCall, J.L. Glass, S.J. Pearton, and R.A. Logan, "Directional light coupling from microdisk laser," Appl. Phys. Lett., 62, 561-563 (1993).
14. R.W. Boyd, and J.E. Heebner, "Sensitive disk resonator photonic biosensor", Appl. Opt., 40, 5742-5747 (2001).
15. D.J.W. Klunder, F.S. Tan, T. van der Veen, H.F. Bulthuis, G. Sengo, B. Docter, H.J.W.M. Hoekstra, and A. Driessen, "Experimental and numerical study of SiON microresonators with air and polymer cladding," J. Lightwave Technol., 21, 1099-1110 (2003).
16. S. Blair and Y. Chen, "Resonant-enhanced evanescent-wave fluorescence biosensing with cylindrical optical cavities", Appl. Opt., 40, 570-582 (2001).
17. Teraoka, S. Arnold, and F. Vollmer, "Perturbation approach to resonance shifts of whispering-gallery modes in a dielectric microsphere as probe of a surrounding medium", J. Opt. Soc. Am. B, 20, 1937-1946 (2003).
18. P.P. Silvester, "Finite element solution of homogeneous waveguide problems", Alta Frequenza, 38, 313-317 (1969).
19. H. Quan and Z. Guo, "Simulation of whispering-gallery-mode resonance shifts for optical miniature biosensors", J. Quantitative Spectroscopy & Radiative Transfer, 93, 231-243 (2005).
20. A. Yariv, Optical electronics in modern communications, 5th ed., Oxford U. Press, Oxford, UK (1997).
21. A. Kovetz, The principles of electromagnetic theory, Cambridge University Press, New York (1990).